Indian Journal of Science and Technology, *Vol 10(21), DOI: 10.17485/ijst/2017/v10i21/114485, June 2017*
ISSN (Print) : 0974-6846
ISSN (Online) : 0974-5645

Crystallographic and Bonding Analysis of 3-(4-Chlorophenyl)-5, 7-dimethoxy-4H-chromen-4-one Holding Spectral and Computational Studies

C. N. Dipuna Das and V. Bena Jothy*

Department of Physics and Research Centre, Women's Christian College, Nagercoil – 629001, Tamil Nadu, India; dipunaabynraj@gmail.com, benaezhil@yahoo.com

Abstract

Objectives: To determine structural properties, thermal properties, hydrogen bonding and charge transfer interactions of title compound experimentally as well as theoretically. **Methods/Statistical Analysis**: Single crystal XRD, Vibrational spectra (FT-IR,FT-Raman, UV-Vis, NMR) compared with computational data using Gaussian'09 program package. Computational analysis such as Normal Co-ordinate Analysis (NCA), Natural Population Analysis (NPA), Natural Bond Orbital Analysis (NBO) predicts charge transfer interactions and hydrogen bonding interactions. **Findings:** Hydrogen bonding revealed from both experimental and computational studies confirms the bioactivity of title compound. Critical parameter in determining electrical transport properties and better antioxidant efficiency is frontier orbital energy gap, which leads to potential activity as a drug candidate. Thermal analysis reveals that this sample can be utilized for opto-electronic and photonic device applications up to 300°C. **Application/Improvements:** Methoxyis of lavoneshave ability to increase lean muscle mass, fat loss in the body and to reduce cortisol levels. Since the title compound is a derivative of is of lavone family, further studies like antioxidant activity, in-silico and in-vitro analysis can be done to confirm whether the title compound can be used for pharmaceutical purpose.

Keywords: NBO, NPA, NMR, TG-DTA, UV-Vis, Vibrational Spectra

1. Introduction

Isoflavones are one of the most potent types of flavonoids, are members of plant polyphenols, and belong to a class of compounds known as flavonoids usually seen in the form of glycosides. They have multi-biological and pharmacological effects because of their potential role in preventing and treating cancer and other human chronic diseases. Owing to their chemical structure, they are weak estrogens well known as phytoestrogens, which help to reduce cardiovascular diseases, protect against prostate problems and osteoporosis by improving bone health[1-4]. The goal of this article is to highlight the results of XRD data supported by vibrational assignments with the aid of Normal Co-ordinate Analysis (NCA), to elucidate Electronic properties, NMR spectra and thermal studies of the title compound.

2. Experimental Details

The title compound 4'-Chloro-5,7-dimethoxyisoflavone / 3-(4-Chlorophenyl)-5,7-dimethoxy-4H-chromen-4-one (4CMIF) with molecular formula $C_{17}H_{13}ClO_4$ and molecular mass 316.72was purchased from BioSyn Research Chemicals Pvt Ltd, Hyderabad (purity 98%). It was recrystallized using chloroform and the data structure of the grown crystal were obtained using BRUKER NONIUS CAD4 single crystal X-ray diffractometer and cell refinement by APEX2/SAINT (Bruker, 2004). FT-IR spectra was recorded in the region 400-4000 cm^{-1}using Perkin Elmer Spectrometer and FT-Raman spectra was recorded in the region 50-4000 cm^{-1} using BRUKER RFS 27 Spectrometer with 1064 nm excitation from Nd: YAG laser source having spectral resolution of ±2 cm^{-1} respectively. UV absorption spectra of the compound were examined in

*Author for correspondence

the range 200-400nm based on ASTME 169-04 using Varian, CARY 100 BIO UV-Visible Spectrophotometer in ethanol and methanol solutions. 1H and 13CNMR spectra of 4CMIF were recorded with the aid of Bruker AVANCE III 500 MHz (AV500) multi nuclei solution NMR Spectrometer. Spectra were obtained directly from pure powdered samples. Thermal analysis was carried out using SDT Q600 V20.9 Build 20 Thermal Analyzer in an inert nitrogen atmosphere within the temperature range of 25 to 900 °C at a heating rate of 10 °C/min.

3. Computational Details

Data collection, reduction and absorption correction were performed by SAINT/XPREP (Bruker, 2004), SIR92, SHELXL2014. ORTEP and Mercury softwares were used for structural analysis. Self-consistent field equation has been solved iteratively to reach the equilibrium geometry corresponding to the saddle point on the potential energy surface (PES). Geometry optimizations and vibrational spectral investigations had been performed using Becke-3- Lee-Yang-Parr (B3LYP) gradient correlation functional with the basis set B3LYP/6-311++G(d,p) using Gaussian'09 program package. Calculated wavenumbers were uniformly scaled and NCA computations using MOLVIB program written by Sundius[5,6]. It have been performed to correlate the calculated frequencies with observed frequencies. To improve agreement between predicted and observed frequencies, a frequency scaled factor of 0.9614 was employed for vibrational analysis[7]. Deviation of experimental value after scaling was found to be less than 10 cm-1 with a few exceptions. Descriptions of predicted frequencies during scaling process were followed by potential energy distribution (PED) matrix and Cartesian representation of force constants were transferred to a non-redundant set of symmetry coordinates, chosen in accordance with the recommendations of Pulay et al.,[8]. NBO calculations were performed using NBO 3.1 program as implemented in the Gaussian'09 package[9]. Considering solvent effect, electronic properties such as HOMO and LUMO energies were determined by DFT approach[10,11]. UV-Vis spectral analysis of 4CMIF was performed by theoretical calculation using Gaussian'09 program package[11,12]. Moreover, changes in thermodynamic functions (heat capacity, entropy, and enthalpy) were assigned for different temperatures from vibrational frequency calculations of the title molecule.

4. Results And Discussions

4.1 X-Ray Crystallography

X-ray data were collected at 300 K using MoKα radiation (λ=0.71073 Å) and for X-ray data collection, a crystal size of 0.300 x 0.300 x 0.250 mm^3 was used. Unit cell

Table 1. Crystal data and structure refinement of 4CMIF

Empirical formula	$C_{17}H_{13}ClO_4$	
Formula weight	316.72	
Temperature	300(2) K	
Wavelength	0.71073 Å	
Crystal system	Monoclinic	
Space group	$P2_1/c$	
Unit cell dimensions	a = 5.3053(3) Å	α= 90°
	b = 20.9803(14) Å	β= 99.352(2)°
	c = 13.2248(7) Å	γ = 90°
Volume	1452.44(15) $Å^3$	
Z	4	
Density (calculated)	1.448 Mg/m^3	
Absorption coefficient	0.279 mm^{-1}	
F(000)	656	
Crystal size	0.300 x 0.300 x 0.250 mm^3	
Theta range for data collection	2.491 to 24.990°.	
Index ranges	-6<=h<=6, -24<=k<=24, -15<=l<=14	
Reflections collected	20397	
Independent reflections	2562 R(int) = 0.0297.	
Completeness to theta = 24.990°	99.9 %	
Absorption correction	Semi-empirical from equivalents	
Max. and min. transmission	0.7461 and 0.6841	
Refinement method	Full-matrix least-squares on F^2	
Data / restraints / parameters	2562 / 0 / 199	
Goodness-of-fit on F^2	1.087	
Final R indices I>2sigma(I).	R1 = 0.0412, wR2 = 0.0899	
R indices (all data)	R1 = 0.0554, wR2 = 0.0990	
Extinction coefficient	n/a	
Largest diff. peak and hole	0.186 and -0.202 $e.Å^{-3}$	

Table 2. Atomic displacement parameters (Å2) for 4CMIF

	U^{11}	U^{22}	U^{33}	U^{12}	U^{13}	U^{23}
C1	0.0483 (13)	0.0446 (13)	0.0282 (11)	0.0015 (11)	0.0012 (10)	0.0056 (10)
C2	0.0369 (12)	0.0377 (12)	0.0407 (13)	0.0027 (10)	0.0001 (10)	0.0029 (10)
C3	0.0430 (13)	0.0417 (13)	0.0366 (12)	0.0068 (10)	0.0086 (10)	-0.0041 (10)
C4	0.0404 (12)	0.0367 (12)	0.0264 (11)	-0.0008 (9)	0.0054 (9)	-0.0024 (9)
C5	0.0350 (11)	0.0337 (11)	0.0244 (10)	-0.0014 (9)	0.0064 (9)	-0.0005 (8)
C6	0.0441 (13)	0.0376 (12)	0.0260 (11)	0.0003 (10)	0.0081 (9)	0.0002 (9)
C7	0.0528 (14)	0.0462 (14)	0.0279 (11)	0.0095 (11)	0.0117 (10)	-0.0018 (10)
C8	0.0339 (11)	0.0382 (12)	0.0237 (10)	-0.0005 (9)	0.0088 (8)	-0.0007 (9)
C9	0.0349 (11)	0.0394 (12)	0.0224 (11)	-0.0032 (9)	0.0074 (9)	-0.0004 (9)
C10	0.0345 (11)	0.0406 (12)	0.0241 (10)	-0.0009 (9)	0.0115 (9)	0.0005 (9)
C11	0.0357 (12)	0.0486 (14)	0.0354 (12)	0.0014 (10)	0.0037 (10)	-0.0090 (10)
C12	0.0426 (13)	0.0409 (13)	0.0467 (13)	-0.0023 (10)	0.0106 (11)	-0.0107 (10)
C13	0.0401 (13)	0.0401 (13)	0.0382 (12)	0.0038 (10)	0.0145 (10)	0.0062 (10)
C14	0.0407 (13)	0.0472 (14)	0.0363 (12)	-0.0005 (11)	0.0004 (10)	0.0040 (10)
C15	0.0418 (13)	0.0367 (12)	0.0330 (11)	-0.0042 (10)	0.0055 (10)	-0.0015 (9)
C16	0.0591 (17)	0.0645 (17)	0.0526 (16)	0.0119 (14)	-0.0124 (13)	0.0074 (14)
C17	0.0522 (15)	0.0714 (17)	0.0323 (12)	0.0120 (13)	0.0140 (11)	-0.0093 (12)
O1	0.0522 (10)	0.0610 (11)	0.0479 (10)	0.0184 (9)	-0.0025 (8)	0.0048 (8)
O2	0.0525 (10)	0.0603 (10)	0.0240 (8)	0.0174 (8)	0.0093 (7)	-0.0030 (7)
O3	0.0544 (10)	0.0675 (11)	0.0217 (8)	0.0179 (8)	0.0044 (7)	-0.0003 (7)
O4	0.0641 (11)	0.0558 (10)	0.0213 (8)	0.0180 (9)	0.0101 (7)	0.0047 (7)
Cl1	0.0573 (4)	0.0466 (4)	0.0723 (5)	0.0120 (3)	0.0102 (3)	0.0074 (3)

parameters of 4CMIF were determined by least-squares technique using many reflections and the structure solved was further refined by full-matrix least squares method using SHELXL97[13]. The intensity data were collected for *h* from -6 to 6, for *k* from -24 to 24 and for *l* from -15 to 14 in the range of 2.491 to 24.990˚ totaling 2562 unique reflections. After so many cycles of refinement, R factor dropped down to 0.0297. Table 1 illustrates the complete crystallographic data and refinement details of 4CMIF molecule that exists in monoclinic system with $P2_1/c$ space group, exhibiting lattice and unit cell parameters α = 90°, β = 99.352(2)°,γ = 90° and a = 5.3053(3) Å, b = 20.9803(14) Å, c=13.2248(7) Å respectively. Values of number of molecules per unit cell (Z) and volume (V) are 4 and 1452.44(15) $Å^3$ respectively. Final anisotropic full-matrix least-squares refinement on F^2 with 199 variables converged at R1 = 4.12%, for the observed data and R2 = 5.54% for all data with goodness-of-fit 1.087 and with gyration radius 4.1331 Å. Value of largest peak in final difference electron density synthesis was 0.186 e/$Å^{-3}$, largest hole was -0.202 e/$Å^{-3}$ and calculated density was 1.448 Mg/m^3. Atomic coordinates (10^{-4}) and equivalent isotropic displacement parameters for 4CMIF, U (eq) defined as traces of the orthogonalized Uijtensor are given in Table 2. Data was subsequently deposited in Cambridge Crystallographic Data Centre [Ref: **CCDC 1490840**].

4.2 Single Crystal XRD Analysis

X-ray crystallography is able to detect the arrangement of atoms within a crystal by the atom-induced diffraction of X-rays. Crystal structure reveals that C-H...O hydrogen bonds connect the different components in three-dimensional network which is given in Table 3.Two hydrogen-bond networks concerned with methyl groups

Table 3. Crystal data of hydrogen bond parameters in 4CMIF

Donor-H… Acceptor	D - H	H...A	D...A	D - H...A	SYMMETRY
C(17)-H(17B)...O(2)	0.93	2.40	3.129(3)	109.5	x,1/2-y,-1/2+z
C(16)-H(16C)...O(1)	0.93	2.40	3.129(3)	109.5	x,1/2-y,-1/2+z
C(15)-H(15)...O(3)	0.93	2.58	3.442(3)	104.3	-1+x,y,z
C(3)-H(3)...O(1)	0.93	2.46	3.442(3)	87.7	-x,1/2+y,1/2-z

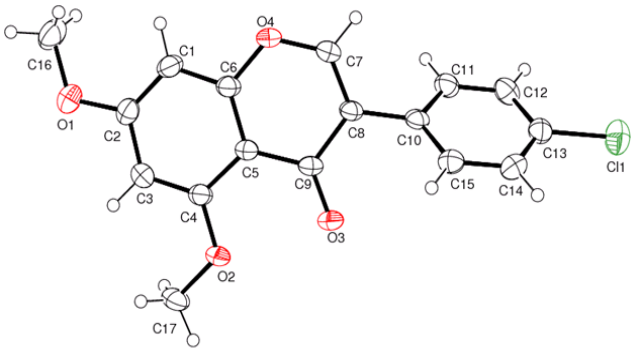

Figure 1. Ortep diagram of 4CMIF.

are O(2)-H(17B) and O(1)-H(16C) having bond angles group which binds to the C(17) (2.40 Å) having bond angle 109.5° with (x,1/2-y,-1/2+z) symmetry. O(3)...H(15) (2.58Å) binds to the carbonyl group of a neighboring molecule with (1+x,y,z) symmetry. C-H_{phenyl} bond is shorter than C-H_{methyl} bond which is due to charge-transfer interaction of the phenyl rings, chlorine atom and methyl group in 4CMIF.Crystallographic structure of 4CMIF obtained by ORTEP is shown in Figure 1.

4.3 Structural Geometry Analysis

Structure optimization of the ground state of 4CMIF have been performed using B3LYP/6-311++G(d,p) basis set. Simulated geometric parameters show good correlations with the crystallographic bond parameters and are summarized in Table 4 and Optimized molecular structure of 4CMIF shown in Figure 2. Calculated C-C bond lengths of 4CMIF C_2-C_3=1.38/1.39Å, C_3-C_4=1.37/1.38Å, C_4-C_5=1.37/1.38Å, C_5-C_6=1.37/1.39Åagrees with the expected[14] region (1.37-1.40Å). Bond length across all rings almost agrees with expected region but elongation happens (C_1-C_{12}=1.48/1.48Å) due to electron delocalization and hyperconjugation. Bond lengths C_{12}-C_{13} and C_{13}-C_{14} increases due to the attachment of carbonyl carbon (C_{13}=O_{18}) and the exception of bond angle C_{12}-C_{13}-C_{14} (114.3°) is due to the conjugation across pyrone ring. Computed values such as bond length C_4-Cl_9=1.78 Å along with bond angles C_3-C_4-Cl_9 and C_5-C_4-Cl_9=119° clearly agrees with the XRD data. C_{14}-C_{13}-O_{18} (124°) is larger than other angles in the rings due to the presence of electron donating oxygen atom. Influence of resonance effect as well as inter electronic interaction effect distorts bond angles in γ-pyrone moiety. Presence of electron donating methyl group affects conjugated double bond system, thereby bonds angles associated with methyl group rises to 109° as electronic charge is back donated from the lone pair oxygen atom to σ* orbital of C-H bonds by elongating C-H bond lengths. C-O-C bond is an electron-attracting group with negative inductive effect (-I) and positive mesomeric effect (+M), so weak hydrogen bonding is observed in chromone part around methoxy group and carbonyl group. Intramolecular hydrogen bonds C_{25}-H_{26}···O_{24}; C_{25}-H_{28}···O_{24} ; C_{31}-H_{34}···O_{30} and C_6-H_{11}···O_{18} have donor-acceptor distances of 2.3Å and 2.1Å (2.7Å)[15,16].revealing weak C-H…O bonding. Dihedral angle between the γ-pyrone ring (A) and the phenyl ring (C) is 43.5°, which indicates phenyl ring with chlorine atom is out of plane with the chromone ring.

4.4 Conformational Analysis

Potential energy surface (PES) scan has been performed to reveal all possible conformations of 4CMIF around C_{17}-C_{12}-C_1-C_6 dihedral angle in order to find the low energy conformer. Different conformers were obtained at steps for every 10° for a 180° rotation around the dihedral angle C_{17}-C_{12}-C_1-C_6, and lowest energy conformer with optimization energy -1416.98 a.u at B3LYP/6-311++G(d,p). Shape of potential energy as a function of dihedral angle is shown in Figure 3. Dihedral angle C_{17}-C_{12}-C_1-C_6 of the optimized conformer having dipole moment 6.6 Debye is 135.6° and 4.7 Debye with 129.3° in single crystal diffraction. In the title compound, coumarin moiety is planar with phenyl ring A attached to C_1 atom but phenyl ring C is twisted from planarity.

4.5 Spectral And Computational Analysis

Theoretical and experimental compared IR and Raman spectra of 4CMIF have been constructed and shown in

Table 4. Optimized Bond lengths (Å), Bond angles (°) and Dihedral angle(°) of 4CMIF by B3LYP/6-311++G(d,p) basis sets along with XRD data

Bond Length	Exp (Å)	Theo. (Å)	Bond angle	Exp(Å)	Theo. (Å)	Dihedral angle (Å)	Exp (Å)	Theo. (Å)
C_1-C_2	1.38	1.40	C_2-C_1-C_6	117.73	118.1779	C_6-C_1-C_2-C_3	-1.07	1.2907
C_1-C_6	1.38	1.40	C_2-C_1-C_{12}	119.94	120.3897	C_6-C_1-C_2-H_7	178.93	-177.1723
C_1-C_{12}	1.48	1.48	C_6-C_1-C_{12}	122.33	121.4277	C_{12}-C_1-C_2-C_3	178.90	-177.9355
C_2-C_3	1.37	1.39	C_1-C_2-C_3	121.65	121.428	C_{12}-C_1-C_2-H_7	-1.10	3.6016
C_2-H_7	0.93	1.08	C_1-C_2-H_7	119.17	119.7067	C_2-C_1-C_6-C_5	2.69	-1.1901
C_3-C_4	1.37	1.38	C_3-C_2-H_7	119.17	118.8478	C_2-C_1-C_{12}-C_{13}	129.29	-136.8953
C_3-H_8	0.93	1.08	C_2-C_3-H_8	120.43	120.703	C_2-C_1-C_{12}-C_{17}	-49.68	43.5014
C_4-C_5	1.37	1.39	C_4-C_3-H_8	120.43	120.305	C_6-C_1-C_{12}-C_{13}	-50.73	43.9041
C_4-Cl_9	1.74	1.76	C_3-C_4-Cl_9	119.41	119.4928	C_6-C_1-C_{12}-C_{17}	130.29	-135.6992
C_5-H_{10}	0.93	1.08	C_5-C_4-Cl_9	119.72	119.533	C_1-C_2-C_3-H_8	179.22	-179.6827
C_6-H_{11}	0.93	1.08	C_4-C_5-H_{10}	120.35	120.0821	H_7-C_2-C_3-C_4	179.22	177.9098
H_{11}-O_{18}	2.60	2.47	C_6-C_5-H_{10}	120.35	120.4447	H_7-C_2-C_3-H_8	-0.78	-1.2069
C_{12}-C_{13}	1.46	1.48	C_1-C_6-C_5	121.25	120.9502	C_2-C_3-C_4-C_5	1.08	-0.2913
C_{12}-C_{17}	1.34	1.34	C_1-C_6-H_{11}	119.37	119.6637	C_2-C_3-C_4-Cl_9	-178.72	-179.7555
C_{13}-C_{14}	1.46	1.48	C_5-C_6-H_{11}	119.37	119.3847	H_8-C_3-C_4-C_5	-178.92	178.829
C_{13}-O_{18}	1.22	1.22	C_{12}-C_{13}-O_{18}	120.94	121.2776	H_8-C_3-C_4-Cl_9	1.28	-0.6353
C_{14}-C_{15}	1.39	1.40	C_{14}-C_{13}-O_{18}	124.46	124.3316	C_3-C_4-C_5-H_{10}	-179.49	-179.5315
C_{14}-C_{20}	1.42	1.42	C_{13}-C_{14}-C_{15}	119.86	120.074	Cl_9-C_4-C_5-C_6	-179.69	179.8489
C_{15}-O_{16}	1.37	1.36	C_{13}-C_{14}-C_{20}	124.66	123.9403	Cl_9-C_4-C_5-H_{10}	0.31	-0.0674
O_{16}-C_{17}	1.34	1.35	C_{15}-C_{14}-C_{20}	115.36	115.9857	C_{20}-C_{21}-C_{22}-O_{30}	179.14	179.9308
C_{17}-H_{19}	0.93	1.08	C_{14}-C_{15}-O_{16}	121.43	121.2774	H_{29}-C_{21}-C_{22}-C_{23}	179.51	179.8375
C_{20}-C_{21}	1.37	1.39	C_{12}-C_{17}-H_{19}	117.72	124.1101	H_{29}-C_{21}-C_{22}-O_{30}	-0.86	-0.1283
C_{20}-O_{24}	1.35	1.34	O_{16}-C_{17}-H_{19}	117.72	110.7205	C_{21}-C_{22}-C_{23}-H_{35}	-179.86	-179.9857
C_{21}-C_{22}	1.39	1.40	C_{20}-C_{21}-C_{22}	120.34	120.1531	O_{30}-C_{22}-C_{23}-C_{15}	179.45	179.9791
C_{21}-H_{29}	0.93	1.07	C_{20}-C_{21}-H_{29}	119.83	119.7435	O_{30}-C_{22}-C_{23}-H_{35}	0.55	-0.0173
C_{22}-C_{23}	1.36	1.38	C_{22}-C_{21}-H_{29}	119.83	120.1034	C_{21}-C_{22}-O_{30}-C_{31}	-175.72	-0.4185
C_{22}-O_{30}	1.35	1.35	C_{15}-C_{23}-H_{35}	121.17	120.666	C_{23}-C_{22}-O_{30}-C_{31}	3.89	179.6143
C_{23}-H_{35}	0.93	1.08	C_{22}-C_{23}-H_{35}	121.17	121.0232	C_{20}-O_{24}-C_{25}-H_{26}	-60.00	-60.8032
O_{24}-C_{25}	1.42	1.42	C_{20}-O_{24}-C_{25}	117.38	119.7658	C_{20}-O_{24}-C_{25}-H_{27}	180.00	-179.3187
C_{25}-H_{26}	0.96	1.09	O_{24}-C_{25}-H_{26}	109.47	111.4112	C_{20}-O_{24}-C_{25}-H_{28}	60.00	62.1937
C_{25}-H_{27}	0.96	1.08	O_{24}-C_{25}-H_{27}	109.47	105.3047	C_{22}-O_{30}-C_{31}-H_{32}	-180.00	-179.748
C_{25}-H_{28}	0.96	1.09	O_{24}-C_{25}-H_{28}	109.47	111.45	C_{22}-O_{30}-C_{31}-H_{33}	-60.00	-61.196
O_{30}-C_{31}	1.35	1.42	H_{26}-C_{25}-H_{27}	109.47	109.4102	C_{22}-O_{30}-C_{31}-H_{34}	60.00	61.7019
C_{31}-H_{32}	0.96	1.08	H_{26}-C_{25}-H_{28}	109.47	109.779			
C_{31}-H_{33}	0.96	1.09	H_{27}-C_{25}-H_{28}	109.47	109.3698			
C_{31}-H_{34}	0.96	1.09	C_{22}-O_{30}-C_{31}	117.59	119.3823			
			O_{30}-C_{31}-H_{32}	109.47	105.6223			
			O_{30}-C_{31}-H_{33}	109.47	111.3386			
			O_{30}-C_{31}-H_{34}	109.47	111.3739			
			H_{32}-C_{31}-H_{33}	109.47	109.3145			
			H_{32}-C_{31}-H_{34}	109.47	109.2973			
			H_{33}-C_{31}-H_{34}	109.47	109.7853			

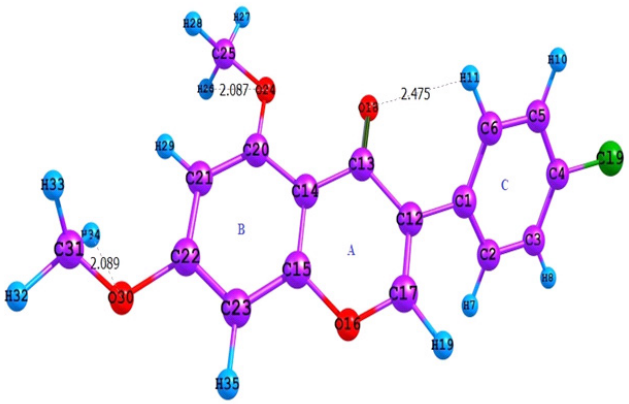

Figure 2. Optimized Molecular Structure of 4CMIF.

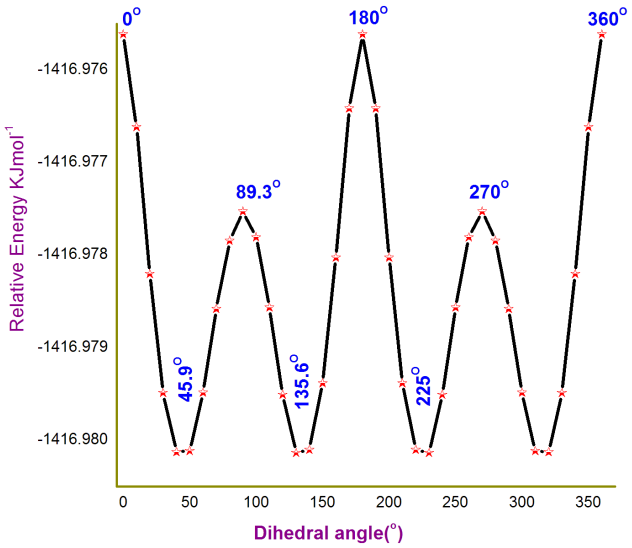

Figure 3. PES Scan for torsional angle C17-C12-C1-C6 of 4CMIF.

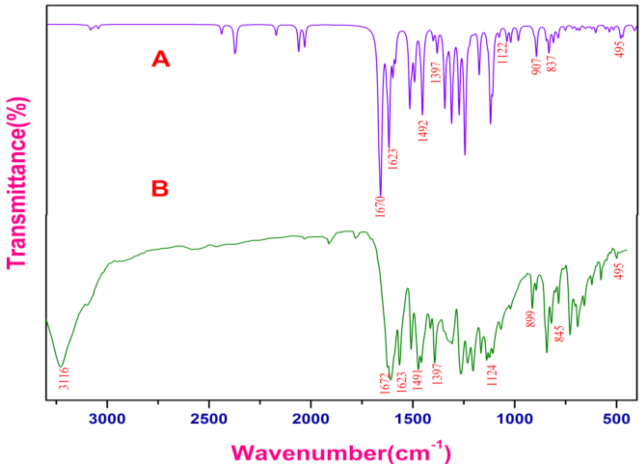

(a)

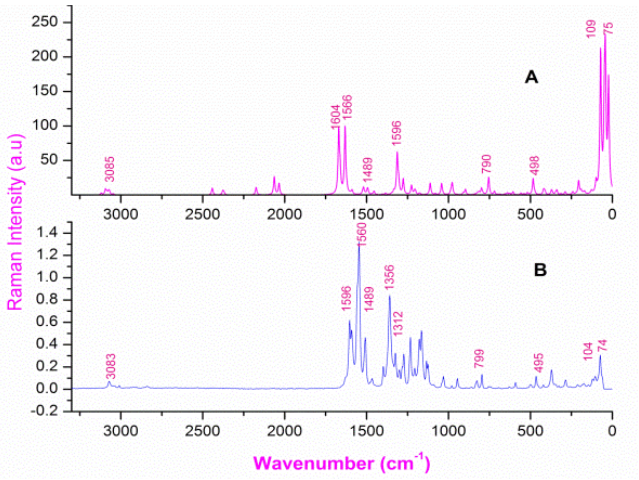

(b)

Figure 4. **(a)** IR Spectra of 4CMIF A) Simulated B) Experimental. **(b)** Raman spectra of 4CMIF A) Simulated B) Experimental.

Figures 4a and 4b. 4CMIF has 35 atoms with heavy 22 atoms and 99 normal modes of vibrations that are distributed amongst the symmetry species as

$$\Gamma_{3N-6} = 67\ \grave{A}\ \text{(in-plane)} + 32\ \hat{A}\text{(out-of-plane)}$$

All vibrations are active in both Infrared absorption and Raman scattering spectra. DFT wave numbers are adjusted by a scaling factor 0.9614 and a non-redundant set of local symmetry coordinates constructed by suitable linear combinations of internal coordinates following the recommendations of[7] are obtained. Detailed vibrational assignments of 4CMIF carried out with the aid of NCA are illustrated in Table 5.

4.5.1 C=O Vibrations

Generally carbonyl stretching vibrations in ketones[17], expected to occur in the region 1715-1680 cm^{-1} are observed as very strong absorption bands at 1670,1623 cm^{-1} in IR and 1629 cm^{-1} in Raman due toC2=O11 stretching. Red shifting of this mode is supported by DFT calculations, which locates these modes at 1670, 1631 cm^{-1} with weak hydrogen bonding as well as resonance stabilized delocalization effect lowering the frequency. Spectral appearance of bands with weak intensity at 689 cm^{-1} in IR and at 419 cm^{-1} in[18] are attributed to deformation bands δC=O usually occurring in IR region 625 ± 70cm^{-1} and Raman region 540 ± 80 cm^{-1}. Sadia Rehman

Table 5. Selected vibrational assignments of 4CMIF by Normal Coordinate Analysis based on SQM force field calculations

Observed fundamentals (cm-1)		Selective scaled B3LYP with 6-31+G(d,P) force field	
ν_{IR}	ν_{Raman}	$\nu_{cal}cm^{-1}$	Assignment (PED%)
3116,Br		3114	νCHIII(99)
	3098,vw	3094	νCH**I** (99)
	3083,vvw	3085	νCH**II** (98)
2456,w		2452	ν_{as}CH**I** (78)
	2432,w	2437	ν_{as}CH**II** (66)
	2034,vw	2034	ν_{ss}CH**II** (97)
2024,vw		2022	ν_{ss}CH**I** (74)
1690,vs		1670	ν_{db}CO**I** (54)
1623,vs	1629,vs	1631	νCC**I** (54),ν_{db}CO**I** (14)
	1181,s	1669	$\beta CHII_{ip}$(77)
1478,s	1468,w	1467	βCHIII $CHII_{SYD}$(52), CHI_{SYD}(26)
1122,m		1123	νCOII (26), ν_MICO (25),ν_MIICO (11)
1112,s	1113,m	1112	νC-ClI(27)
104,w			
74,s			

vs: verystrong; s: strong; m: medium; w: weak; υ: stretching; β: bending; db: double bond;ν:stretching;β:bending;M:methylgroup

et al assigned weak band in the range of 1090-1120 cm^{-1} as the stretching frequency of C-O of lactone ring [19]and as such1122 cm^{-1}(IR) medium bands and 1123 cm^{-1} with PED (26%) are assigned to νC-O mode.

4.5.2 C-H Vibrations

C-H stretching modes usually appear with strong Raman intensity and are highly polarized and give rise to multiple band[20-21]in the region 3100-3000 cm^{-1} and a blue shift in frequency at 3116 cm^{-1} is observed in IR spectrum with computed value at 3114 cm^{-1}. C-H stretching vibrations occur as strong Raman band at 3085 cm^{-1} (98%) and very strong IR band at 3098cm^{-1} (99%) and 3046cm^{-1} (99%). In-plane aromatic C-H bending vibrations appear in the range 1400-1000 cm^{-1}.In 4CMIF, C-H bending vibrations are observed as strong bands at 1334, 1234, 1204 and 1082 cm^{-1} in FT-IR and as medium bands at 1384, 1232, 1205 cm^{-1} in Raman.

4.5.3 Methoxy Group Vibrations

Electronic effects such as mesomeric effect can shift C-H stretching and bending bands if CH_3 group attaches to an oxygen atom[22]. O-CH_3 stretching band is red shifted to 2024 cm^{-1}(IR) and 2034 cm^{-1}(Raman) which are assigned to methoxy symmetric stretching modes[23]which usually occur in the region 3000-2815cm^{-1}. Weak bands at 2456 cm^{-1} in IR and at 2432 cm^{-1} in Raman attributed to asymmetric stretching modes on the other hand asymmetric bending vibrations of methoxy groups[23-24]normally appearing at 1500-1450 $cm^{-1}$are observed as strong bands at 1478 cm^{-1} in IR and weak band at 1468cm^{-1} in Raman. Moreover, rocking vibration of the CH_3 group in DMIF appears as mixed vibrations. Computed values reveal that the predicted very strong intensity band at 1181cm^{-1} in Raman, is strongly coupled with aromatic C-H in-plane bending mode, CH_3 rock and C-O stretch. This increases the conjugation inside Phenyl ring A and calculated hyper conjugative interactions [$LP_1O_{30} \rightarrow \sigma^*$ (C_{31}-H_{32}); $LP_1O_{30} \rightarrow \sigma^*$ (C_{31}-H_{34}); $LP_2O_{30} \rightarrow \sigma^*$ (C_{31}-H_{34}); $LP_1O_{24} \rightarrow \sigma^*$ (C_{25}-H_{26}); $LP_2O_{24} \rightarrow \sigma^*$ (C_{25}-H_{28}); $LP_1O_{30} \rightarrow \sigma^*$ (C_{21}-H_{29})] supports weak electrostatic C-H…O intra-molecular hydrogen bonding interactions[25.]

4.5.4 C-Cl Vibrations

Vibrations of C-X group (X=Cl, Br, I) are assigned by[26.]in the frequency range 1129-480 cm^{-1}. In the experimental spectra, C-Cl stretching vibrations are observed as very strong band at 1112 $cm^{-1}$and as medium band at 1113cm^{-1}in IR and Raman respectively. C-Cl out-of-plane bending vibrations are observed at 313cm^{-1}in FT-Raman spectra that are supported by literature [27-28].

4.5.5 Ring Vibrations

ν(C=C) vibration mode occurs in the spectral region around 1655 cm^{-1} for 4H-chromene[29] and a very strong band at 1629cm^{-1} visualized in IR spectra is assigned to it. Ring C-C vibrations are expected to occur in the range 1600-1400 cm^{-1} which are observed in IR and Raman spectra as strong bands at 1605 and 1604 cm^{-1} and DFT value predicts this at 1601 cm^{-1} with PED (49%).

4.5.6 Lattice Mode Vibrations

DFT calculation reveals that certain low frequency Raman band arises from lattice mode vibrations[30-34]found below 150 cm^{-1}. The lattice mode vibrations observed

in Raman at 104 cm^{-1} as very weak band and at 74cm^{-1} as strong band are associated with C_6-C_5-C_4-C_{19}, C_2-C_3-C_4-C_{19}, C_4-C_{19}-C_{20}-C_{24} torsional modes.

4.6 Bonding Analysis

4.6.1 Global Aromaticity

Global aromaticity indicators include the Highest Occupied Molecular Orbital (HOMO) and Lowest Unoccupied Molecular Orbital (LUMO) gap as it directly relates the ability of molecule to undergo chemical reactions. The larger the gap, the least (energetically) accessible is the LUMO orbital and thus, the least reactive molecule should have an extra-energy stabilization characteristic of aromatic molecules. Molecular orbital plots of the frontier orbitals for the ground state of 4CMIF molecule including HOMO, LUMO, LUMO+1, LUMO+2 computed at B3LYP/6-311++G(d,p) level are shown in Figure 5. In 4CMIF, HOMO and HOMO-1 are located on oxygen atoms connecting methyl groups, chlorine atom in phenyl ring C and carbonyl group while HOMO-2 is localized on γ-pyrone moiety. LUMO populates on bonded carbon-oxygen atoms (C_{15}-O_{16}, C_{17}-O_{16}, C_{20}-O_{24}, C_{22}-O_{30}) and carbonyl group. However, in LUMO+1 minor population is around the carbons atoms of Phenyl rings A,B and C. In LUMO+2 majority populates around the carbon atoms in ring C and ring B. Energy values of LUMO, HOMO and their energy gap reflect the chemical activity and possibility of intramolecular charge transfer analysis as well as bioactivity confirmation of the molecule[35]. Optimized electronic energy of 4CMIF is -6.17J and the critical parameter in determining electrical transport properties and better antioxidant efficiency is frontier orbital energy gap (E_{HOMO}–E_{LUMO}) is found to be -4.58 eV[26]. (HOMO-1)- (LUMO+1) and (HOMO-2)-(LUMO+2) energy gap values are -5.46 eV and -6.02 eV respectively which is tabulated in Table 6.

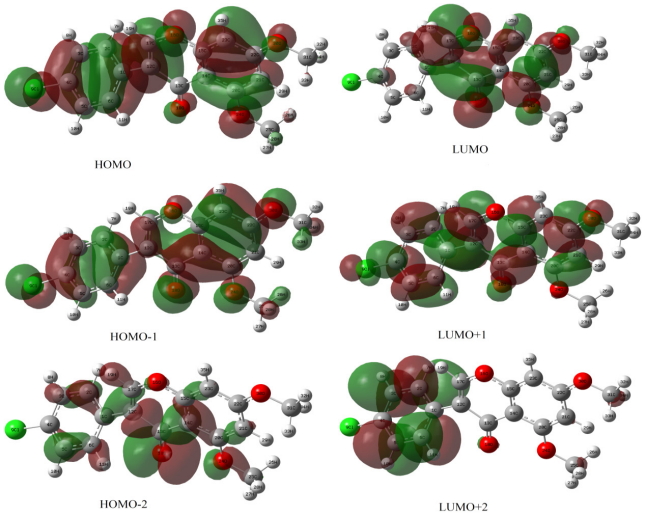

Figure 5. HOMO-LUMO plot of 4CMIF.

4.6.2 Natural Population Analysis

Population analysis is a technique in computational chemistry that assigns an average number of electrons, the atomic population, to each atom in a molecule. Natural atomic charges and orbital populations of molecular wave functions in atomic orbital basis sets can be analyzed by Natural Population Analysis. As oxygen is electronegative, it draws electrons in bonds and shares with hydrogen atoms so that hydrogen atoms left with net positive charges. Charge distributions of optimized monomer 4CMIF mark out that all hydrogen atoms possess positive charge and among them H_{11} possess highest positive charge due to intramolecular bonding interaction sites. All oxygen atoms acquires negative charge while carbonyl oxygen atom (O_{18}) have highest negative charge attached to positive carbon atom C_{13} forming strong hydrogen bonding interactions.

Table 7 lists out the summary of natural population charges from NBO output and Figure 6 shows natural population atomic charges of 4CMIF.

4.6.3 Natural Hybrid Orbital (NHO) Directionality Analysis

Natural Hybrid directionality provides hints of angular deformations in nonplanar torsional geometries and steric effect. Table 8 provides the bending angles of different

Table 6. Calculated Energy Values of 4CMIF in Gas Phase

B3LYP/6-31+G(d,p)	Values
Optimized Electronic Energy(Hartree)	-1416.98
HOMO(eV)	-6.19
LUMO(eV)	-1.61
HOMO-LUMO Energy Gap(eV)	-4.58
HOMO-1(eV)	-6.62
LUMO+1(eV)	-1.16
HOMO-1- LUMO+1 Energy Gap(eV)	-5.46
HOMO-2(eV)	-6.66
LUMO+2(eV)	-0.641
HOMO-2 -LUMO+2 Energy Gap(eV)	-6.02
Dipole moment (Debye)	6.6051

Table 7. Summary of natural population charges from NBO output

Atom	Electronic ConFigureuration	NPA
C_1	$2S^{0.86}2p^{3.18}4p^{0.02}$	-0.053
C_2	$2S^{0.93}2p^{3.22}4p^{0.01}$	-0.166
C3	$2S^{0.95}2p^{3.27}4p^{0.01}$	-0.233
C_4	$2S^{0.93}2p^{3.08}3d^{0.01}4p^{0.01}$	-0.034
C_5	$2S^{0.95}2p^{3.26}4p^{0.01}$	-0.228
C_6	$2S^{0.93}2p^{3.19}4p^{0.01}$	-0.14
H_7	$1S^{0.79}$	0.206
H_8	$1S^{0.78}$	0.2201
Cl_9	$3S^{1.84}3p^{5.15}3d^{0.01}4p^{0.01}$	-0.004
H_{10}	$1S^{0.78}$	0.2209
H_{11}	$1S^{0.77}$	0.2279
C_{12}	$2S^{0.91}2p^{3.26}4p^{0.01}$	-0.195
C_{13}	$2S^{0.79}2p^{2.65}3d^{0.01}4p^{0.03}$	0.5134
C_{14}	$2S^{0.90}2p^{3.33}4p^{0.01}$	-0.248
C_{15}	$2S^{0.82}2p^{2.79}3d^{0.01}4p^{0.01}$	0.3671
O_{16}	$2S^{1.57}2p^{4.89}3p^{0.01}$	-0.48
C_{17}	$2S^{0.90}2p^{2.85}3d^{0.01}4p^{0.01}$	0.2278
O_{18}	$2S^{1.69}2p^{4.87}3p^{0.01}$	-0.572
H_{19}	$1S^{0.80}$	0.1953
C_{20}	$2S^{0.80}2p^{2.76}3^{0.01}3d^{0.01}4p^{0.01}$	0.4142
C_{21}	$2S^{0.94}2p^{3.44}4p^{0.01}$	-0.389
C_{22}	$2S^{0.82}2p^{2.79}3d^{0.01}4p^{0.01}$	0.3734
C_{23}	$2S^{0.94}2p^{3.35}4p^{0.01}$	-0.313
O_{24}	$2S^{1.58}2p^{4.90}3p^{0.01}$	-0.504
C_{25}	$2S^{1.07}2p^{3.11}3p^{0.01}3d^{0.01}$	-0.198
H_{26}	$1S^{0.83}$	0.1684
H_{27}	$1S^{0.80}$	0.1988
H_{28}	$1S^{0.83}$	0.1681
H_{29}	$1S^{0.78}$	0.2191
O_{30}	$2S^{1.59}2p^{4.93}3p^{0.01}$	-0.531
C_{31}	$2S^{1.08}2p^{3.11}3p^{0.01}3d^{0.01}$	-0.207
H_{32}	$1S^{0.80}$	0.1963
H_{33}	$1S^{0.83}$	0.1716
H_{34}	$1S^{0.83}$	0.1714
H_{35}	$1S^{0.76}$	0.2348

bonds expressed as angle of deviation from the direction of the line joining the two nuclei centers. The bent $\sigma(O_{30}–C_{22})$ of bond orbital from the line of O-C centers decreases (1.9°) due to the presence of methyl group close

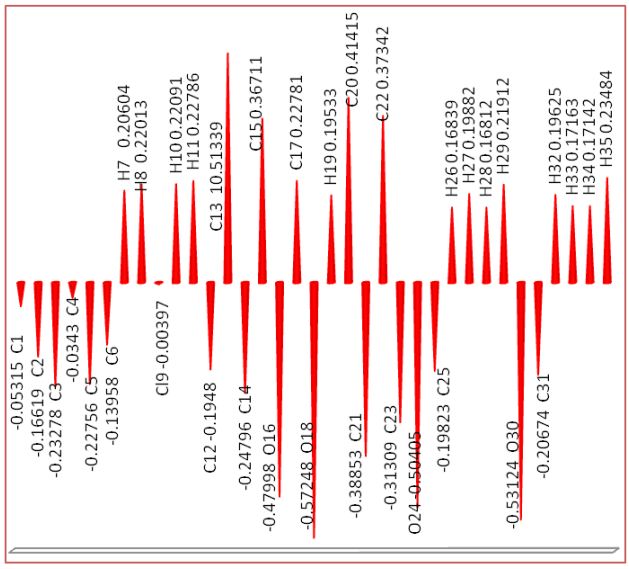

Figure 6. Natural population atomic charges of 4CMIF.

Table 8. NHO directionality and bond bending of 4CMIF

	Line of Centers		Hybrid 1			Hybrid 2		
BondA-B	θ	φ	Θ	φ	Dev	θ	φ	Dev
σC_{13}-O_{18}	88.4	108.0	87.1	107.8	1.4	90.3	288.9	1.5
σC_{12}-C_{17}	95.0	290.0	90.6	290.8	4.4	80.6	106.5	5.6
σC_{22}-O_{30}	90.4	337.3	90.0	342.1	4.8	89.5	155.4	1.9
σC_{20}-O_{24}	85.4	103.1	85.3	99.4	3.7	94.6	284.7	1.6
σC_1-C_{12}	92.3	350.4	-	-	-	88.0	169.3	1.2
σC_1-C_2	55.7	224.6	57.3	227.0	2.6	126.4	44.9	2.1
σC_1-C_6	121.7	120.1	122.0	118.4	1.5	-	-	-
σC_{14}-C_{15}	94.1	283.9	94.1	282.6	1.3	85.9	107.4	3.5

to it while, O_1 NHO of $\sigma(O_{24}–C_{20})$ bond orbital shows a large deviation of 3.7° resulting in the strong charge transfer path towards electron rich oxygen atoms O_{24} and O_{30}. Carbon NHO of σ has 65.07% p character ($SP^{1.88}$) bent away from the line of C_{12}-C_{17} centers by 4.4° due to steric repulsion effect around these centers. While orienting to coplanar, lower bending effect precedes at γ-pyrone moiety junction C_1-C_{12} (1.2°) but attached phenyl ring has carbon NHOs of bonds C_1-C_2 and C_1-C_6 showing deviations from the line of nuclear centers by (2.5°). Vicinal bonded ring oxygen atom slightly bent as $\sigma(C_{14}$-$C_1)$ bond is minimized by 1.3°.

Table 9. Second order perturbation analysis of Fock matrix using NBO basis of 4CMIF

Donor (i)	ED E (e)	Acceptor (j)	ED(j) (e)	E (2)[a] (kJ/mol)	E(j)- E(i)[b] (a.u)	F(i.j)[c] (a.u)
LP_3Cl_9	1.93031	π^*C_3-C_4	0.39432	13.32	0.30	0.062
LP_2O_{16}	1.74746	π^*C_{12}-C_{17}	0.18537	30.49	0.38	0.098
LP_2O_{16}	1.74746	π^*C_{15}-C_{23}	0.40485	24.48	0.37	0.089
LP_2O_{18}	1.88026	σ^*C_{12}-C_{13}	0.07018	18.70	0.73	0.105
LP_2O_{18}	1.88026	σ^*C_{13}-C_{14}	0.06405	24.94	0.56	0.107
LP_2O_{24}	1.80793	π^*C_{14}-C_{20}	0.47924	33.43	0.33	0.102
LP_2O_{18}	1.88026	σ^*C_6-H_{11}	0.01277	12.24	0.21	0.045
LP_1O_{24}	1.96156	σ^*C_{25}-H_{26}	0.01799	5.67	0.21	0.031
LP_2O_{24}	1.80793	σ^*C_{25}-H_{28}	0.01808	7.29	2.46	0.125
LP_1O_{30}	1.96264	σ^*C_{31}-H_{32}	0.00872	2.01	2.83	0.068
LP_1O_{30}	1.96264	σ^*C_{31}-H_{34}	0.01787	0.78	2.51	0.040
LP_2O_{30}	1.83170	π^*C_{21}-C_{22}	0.44852	32.07	0.35	0.102
LP_2O_{30}	1.83170	σ^*C_{31}-H_{34}	0.01787	1.51	2.28	0.054
LP_1O_{30}	1.96264	σ^*C_{21}-H_{29}	0.01487	1.01	1.01	0.029
σC_1-C_2	1.96923	σ^*C_1-C_6	0.02601	9.74	0.55	0.065
σC_1-C_{12}	1.96477	σ^*C_1-C_6	0.02601	12.82	0.51	0.072
πC_1-C_2	1.96923	π^*C_3-C_4	0.39432	23.66	0.24	0.068
πC_1-C_2	1.96923	π^*C_5-C_6	0.30265	19.82	0.28	0.067
σC_2-H_7	1.97899	σ^*C_1-C_6	0.02601	40.56	0.38	0.111
σC_3-C_4	1.97949	π^*C_1-C_2	0.36587	17.52	1.05	0.133
σC_3-C_4	1.97949	π^*C_3-C_4	0.39432	14.13	1.06	0.121
πC_3-C_4	1.68213	π^*C_1-C_2	0.36587	33.41	0.26	0.083
πC_3-C_4	1.68213	σ^*C_1-C_6	0.02601	30.20	0.13	0.061
πC_3-C_4	1.68213	π^*C_5-C_6	0.30265	15.37	0.30	0.061
σC_4-Cl_9	1.98870	π^*C_3-C_4	0.39432	16.11	1.04	0.129
σC_5-C_6	1.96731	σ^*C_1-C_6	0.02601	21.98	0.56	0.099
πC_5-C_6	1.65941	π^*C_1-C_2	0.36587	24.12	0.23	0.067
πC_5-C_6	1.65941	π^*C_3-C_4	0.39432	24.85	0.24	0.069
σC_5-H_{10}	1.97828	σ^*C_1-C_6	0.02601	16.53	0.38	0.071
σC_6-H_{11}	1.97800	σ^*C_1-C_6	0.02601	179.49	0.44	0.251
σC_6-H_{11}	1.97800	π^*C_{13}-O_{18}	0.25852	138.91	0.22	0.166
σC_{12}-C_{13}	1.96927	σ^*C_1-C_6	0.02601	23.26	0.52	0.098
σC_{12}-C_{13}	1.96927	π^*C_{13}-O_{18}	0.25852	17.06	0.30	0.068
σC_{12}-C_{17}	1.98095	σ^*C_1-C_6	0.02601	14.63	0.63	0.086
σC_{14}-C_{15}	1.97180	π^*C_{13}-O_{18}	0.25852	67.58	0.36	0.149
σC_{14}-C_{15}	1.97180	σ^*C_{23}-H_{35}	0.01170	92.29	0.08	0.075
σC_{14}-C_{20}	1.96399	π^*C_{13}-O_{18}	0.25852	23.96	0.34	0.085
πC_{14}-C_{20}	1.58344	π^*C_{15}-C_{23}	0.40485	30.05	0.27	0.081
σC_{15}-O_{16}	1.98955	σ^*C_{13}-C_{14}	0.06405	12.09	1.26	0.112
σC_{15}-C_{23}	1.97120	σ^*C_{13}-C_{14}	0.06405	36.86	1.09	0.181
σC_{15}-C_{23}	1.97120	σ^*C_{14}-C_{15}	0.02853	14.30	1.30	0.122
σC_{15}-C_{23}	1.97120	σ^*O_{16}-C_{17}	0.02048	30.96	0.98	0.156
σC_{15}-C_{23}	1.97120	σ^*C_{22}-C_{23}	0.01988	23.91	1.20	0.152
σC_{15}-C_{23}	1.97120	σ^*C_{23}-H_{35}	0.01170	983.10	0.12	0.309
πC_{15}-C_{23}	1.67864	π^*C_{14}-C_{20}	0.47924	13.07	0.28	0.056
πC_{15}-C_{23}	1.67864	π^*C_{21}-C_{22}	0.44852	26.60	0.29	0.081
σC_{21}-C_{22}	1.97517	σ^*C_{23}-H_{35}	0.01170	868.44	0.04	0.167
σC_{22}-C_{23}	1.96897	σ^*C_{21}-C_{22}	0.02888	11.86	1.34	0.113
σC_{22}-C_{23}	1.96897	σ^*C_{22}-C_{23}	0.01988	48.45	1.25	0.220
σC_{22}-C_{23}	1.96897	σ^*C_{23}-H_{35}	0.01170	882.37	0.17	0.347
σC_{22}-O_{30}	1.99195	σ^*C_{23}-H_{35}	0.01170	59.17	0.19	0.094
σC_{23}-H_{35}	1.97368	σ^*C_{14}-C_{15}	0.02853	14.11	0.64	0.085
σC_{23}-H_{35}	1.97368	σ^*O_{16}-C_{17}	0.02048	67.63	0.31	0.130
σC_{23}-H_{35}	1.97368	σ^*C_{21}-C_{22}	0.02888	12.57	0.63	0.079
σC_{23}-H_{35}	1.97368	σ^*C_{22}-C_{23}	0.01988	25.38	0.53	0.104
σC_{23}-H_{35}	1.97368	σ^*C_{25}-H_{28}	0.01808	26.47	2.24	0.218
σC_{23}-H_{35}	1.97368	σ^*C_{31}-H_{32}	0.00872	27.14	2.37	0.228

4.6.4 *Natural Bond Orbital Analysis*

NBO data holds electron density transfer between lone pair of electron donor atom to acceptor orbitals treated with second-order perturbation theory analysis to expound the intra-molecular bonding, re-hybridization and delocalization of electron density within the molecule [36] which has been performed at the DFT/B3LYP/6-311++G(d,p) level. NBO analysis reveals that charge transfer from methyl group to ring system and hyperconjugative interactions associated with hybrid orbital C_{31}-H_{32}, C_{31}-H_{34}, C_{25}-H_{26} and C_{25}-H_{28} are due to the overlapping of sp and $sp^{1.68}$ hybrid on O30 as well as sp and $sp^{1.69}$ hybrid on O24. [$LP_1O_{30} \rightarrow \sigma^*$ (C_{31}-H_{32}); $LP_1O_{30} \rightarrow \sigma^*$ (C_{31}-H_{34}); $LP_2O_{30} \rightarrow \sigma^*$ (C_{31}-H_{34}); $LP_1O_{24} \rightarrow \sigma^*$ (C_{25}-H_{26}); $LP_2O_{24} \rightarrow \sigma^*$ (C_{25}-H_{28}); $LP_1O_{30} \rightarrow \sigma^*$($C_{21}$-$H_{29}$)] magnifies weak electrostatic C-H…O intra-molecular hydrogen bonding[36]. Higher electronegativity reflects larger polarization coefficients across methoxy groups and the linear combination of its constituent natural hybrid orbitals are

$$\sigma O_{24}C_{20} = 0.5714(sp^{3.06}) + 0.8206(sp^{1.89})$$

$$\sigma O_{30}C_{22} = 0.5691(sp^{3.04}) + 0.8223(sp^{1.93})$$

NBO analysis reveals no significant charge transfer between the halogen lone pairs. Table 9 shows second order perturbation analysis of Fock matrix using NBO basis of 4CMIF.

4.7 Molecular Electrostatic Potential Surface Analysis

Electrostatic potential maps are very useful three-dimensional diagrams of molecules that enable us to visualize the charge distributions of molecules and charge related properties of molecules. Electrostatic potential energy data is easy to interpret as it is a color spectrum obtained using Gaussian with red as the lowest electrostatic potential energy and blue as the highest electrostatic potential energy values[37]. Positive, neutral and negative electrostatic potential regions are shown in terms of color grading in the order red < orange < yellow < green < blue[38,39]. In 4CMIF, ring carbon atoms are bluish green in color but electrophilic carbon atoms that are coupled together with oxygen atoms show red color confirming hydrogen bonding interactions. Negative (red) potential is most prominent above the double bonds and covers carbonyl oxygen atom with a value of -0.635 a.u, the maximum negative density resides directly above the center of the molecule. Total electron density and isocontour images of 4CMIFare shown in Figures 7a and 7b.

4.8 UV-Vis Spectral Analysis

Isoflavones exhibit an intense B and II absorption with only a shoulder or low intensity peak representing Band I UV absorption[40]. UV-vis Spectra of 4CMIF was measured in different solvents such as methanol and ethanol as shown in Figure 8. In the present work, TDDFT calculations were carried out in all solvents using B3LYP/6-311++G (d,p) method to predict electronic excitation energies. Spectra of all solutions show intense broad and wide absorption bands and their peak positions are sensitive to solvent polarity. Band II UV

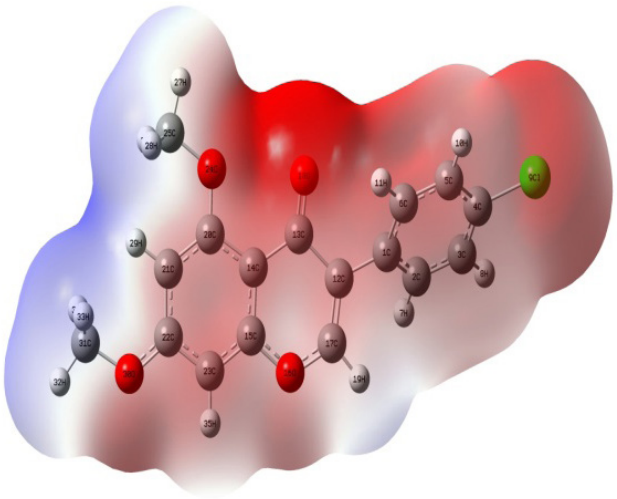

(a)

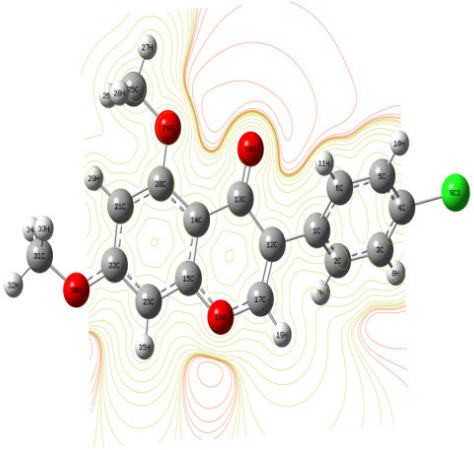

(b)

Figure 7. **(a).** Electron Density Map of 4CMIF, **(b).** Isocontour Map of 4CMIF.

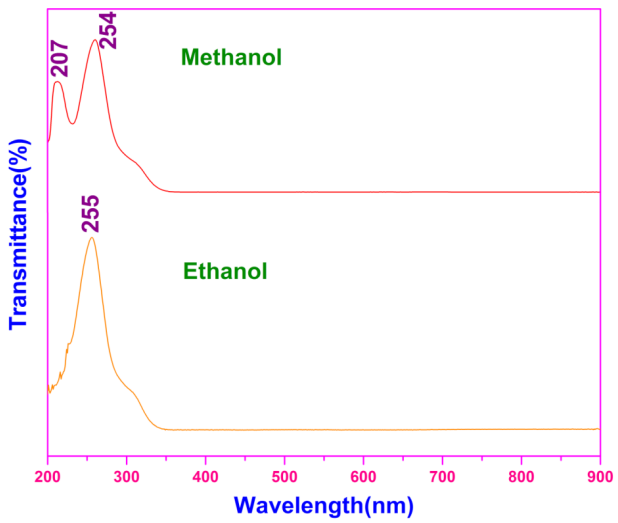

Figure 8. UV-Vis Spectra of 4CMIF using methanol and ethanol solvents.

absorption usually occurs in the region 240-285nm[41]. Electronic transition from HOMO→LUMO having ≈ 54% contribution shows ≈ 264nm in both solutions and theoretically interpretsat 254 and 255 nm for methanol and ethanol respectively. Weak n→π* transition around carbonyl chromophore is shifted to 200-215 nm[41-42]which is due to hydrogen bonding showing low intensity peak at 207nm in γ-pyrone moiety for methanol solvent with f = 0.0306 oscillator strength. Experimental peaks along with calculated excitation energies; absorbance and oscillator strength (f) for the title compound are compared for methanol and ethanol solvents and tabulated in Table 10.

Table 10. UV-Vis excitation energy and oscillator strength of 4C57DMIF for Methanol and Ethanol solvents calculated by TDDFT/B3LYP/6-311++G(d,p) method

No.	Wave length(nm)		Energy (ev)	Osc. Strengh	Symmetry	Major contributes
	Exp.	Cal.				
Solvent : **Methanol**						
1		318	3.89	0.0016	Singlet-A	H-2->LUMO (83%)
2		314	3.93	0.082	Singlet-A	HOMO->LUMO (94%)
3		286	4.32	0.1384	Singlet-A	HOMO->L+1 (70%)
4		274	4.51	0.329	Singlet-A	H-1->LUMO (69%)
5	254	264	4.67	0.5366	Singlet-A	H-3->LUMO (52%)
6	207	261	4.74	0.0306	Singlet-A	HOMO->L+2 (46%)
Solvent : **Ethanol**						
1		318	3.89	0.0014	Singlet-A	H-2->LUMO (85%)
2		314	3.94	0.0835	Singlet-A	HOMO->LUMO (94%)
3		286	4.32	0.143	Singlet-A	HOMO->L+1 (71%)
4		274	4.51	0.343	Singlet-A	H-3*LUMO (97%)
5		265	4.67	0.5313	Singlet-A	H-3->LUMO (54%)
6	255	261	4.74	0.0314	Singlet-A	HOMO->L+2 (45%)

4.9 NMR Analysis

Nuclear magnetic resonance spectroscopy is a powerful analytical technique used to characterize organic molecules by identifying carbon-hydrogen frameworks within molecules using ^{1}H NMR and ^{13}C NMR analysis. Gauge-Invariant Atomic Orbitals (GIAO) calculations were performed using DFT/B3LYP with 6-311++G (d,p) level basis set. NMR solvent Deutero chloroform $CDCl_3$is liable to dissolve compounds of reasonably varying polarity.

4.9.1 ^{1}H NMR Spectral Analysis

^{1}H NMR spectrum absorption region for common organic solvents in $CDCl_3$ is around δ 6.0 to 7.9 ppm[43]. Chemical shift for protons attached to the ring C appears in the range δ= 7.79 ppm and the experimental values to some extent fall in the same range coinciding with the theoretical data. Among all protons in the title compound, H_{19} acquires high chemical shift value and as a result, resonance occurs at lower applied field. Intramolecular hydrogen bonds in six-membered ring generally display a very low-field resonance[44]. Increasing electronegativity of the group bonded to methyl group deshields nearby hydrogen H_{35} resulting in a downfield shift of δ=6.7 ppm. Proton associated with methyl group via oxygen atom -O-CH3resonate at lower field and absorption region around δ=3.3ppm due to C_{31}-H_{34}…O_{30} intramolecular hydrogen bonding.

4.9.2 CMR Spectral Analysis

In ^{13}CNMR (CMR) chemical shifts are extremely sensitive to substitution and molecular geometry. CMR spectra

appear between low field carbonyl carbons and high field methyl carbons in the range δ 0-200 ppm[43]. In phenyl ring A, sp^2 hybridized C_{14} due to resonance effect of adjacent carbonyl group $C_{13}=O_{18}$ absorbs downfield having chemical shift δ=109.7ppm[44]. Meanwhile C_{13} of carbonyl group absorbs far downfield exhibiting highest chemical shift of δ=174.9 ppm. Methyl carbon peak appears at δ = 55.7ppm but attachment of electronegative atom to carbon bearing proton causes a downward shift[43]and hydrogen bonding C_{31}-H_{34}…O_{30};C_{25}-H_{26}…O_{24};C_{25}-H_{28}…O_{24}. decreases the electron density around the proton causing deshielding to move the proton absorption to lower field with lower chemical shift values around δ=3.9 ppm.

Table 11 shows solvent induced shifts relative to chloroform $CDCl_3$calculated experimentally and theoretically. Figures 9a and 9b show the experimental ^{13}C and ^{1}H NMR spectra.

4.10 Thermo Gravimetric (TG) and Differential Thermal Analysis (DTA)

Thermo gravimetric (TG) and differential thermal analysis (DTA) of 4CMIF were carried out using SDT Q600 V20.9 Build 20 Thermal Analyzer in an inert nitrogen atmosphere in the region 30-500°C at a heating rate of 10°C per minute in nitrogen atmosphere. When the sample was heated beyond 300°C, it was observed to undergo two stages of decomposition, which confirm the presence of different chromophores in crystal lattice.

TGA curve shows that the material is stable up to 300°C and it is decompose around 380°C. In DTA, the first endothermic peak obtained at 194°C indicates the

Table 11. Experimental and theoretical 13C and 1H isotropic chemical shifts of 4CMIF

^{13}C NMR	Experimental	Theoretical	^{1}H NMR	Experimental	Theoretical
	Solvent Chloroform	Solvent Chloroform		Solvent Chloroform	Solvent Chloroform
C_1	130.5	134.1	H_7	7.42	7.5
C_2	128.4	129.7	H_8	7.6	7.5
C_3	128.4	129.4	H_{10}	7.5	7.3
C_4	133.9	143.8	H_{11}	7.47	7.42
C_5	125.3	128.9	H_{19}	7.76	7.75
C_6	130.4	134.1	H_{26}	3.87	3.83
C_{12}	125.3	129.7	H_{27}	4.49	4.8
C_{13}	174.9	173.9	H_{28}	3.9	3.8
C_{14}	109.7	110.3	H_{29}	6.2	6.3
C_{15}	159.9	162.8	H_{32}	4.2	3.9
C_{17}	150.6	153.2	H_{33}	3.9	3.9
C_{20}	161.5	161.8	H_{34}	3.9	3.9
C_{21}	77.4	78.6	H_{35}	6.7	6.4
C_{22}	164.1	166.8			
C_{23}	96.3	96.9			
C_{25}	56.3	55.5			
C_{31}	55.7	55.5			

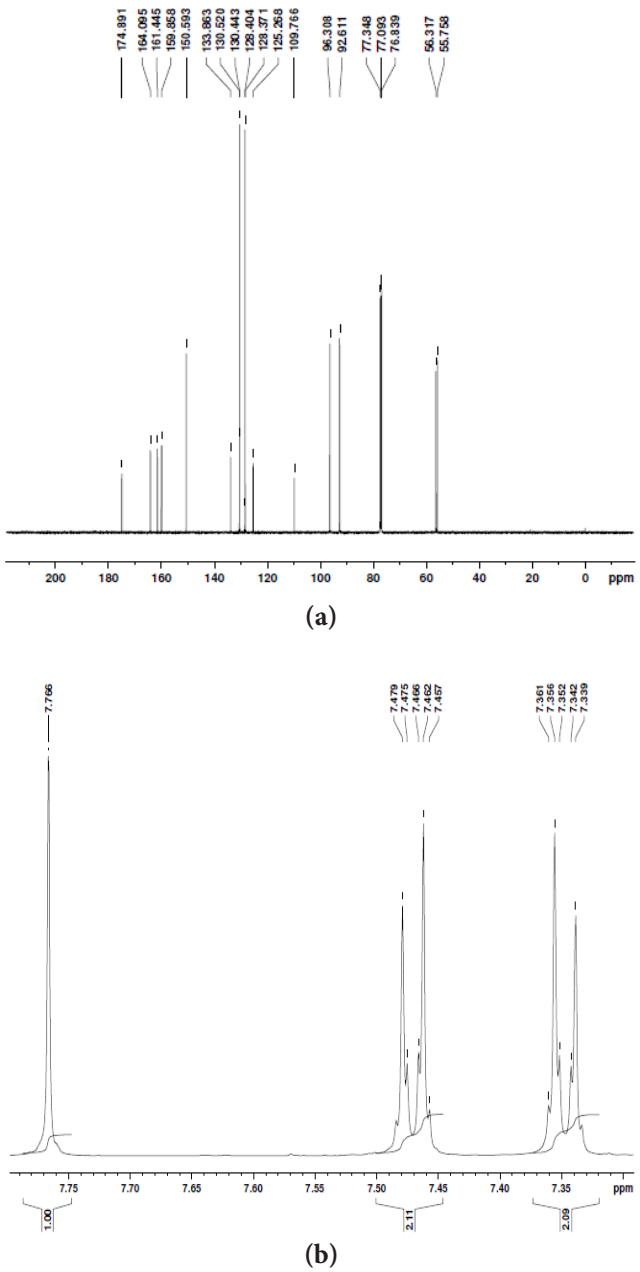

Figure 9. **(a)** ^{13}CMR Spectra of 4CMIF, **(b)** 1H NMR Spectra of 4CMIF.

absence of physically absorbed or lattice water in the crystal. A second peak seen at 370°C shows the decomposition of the crystal and this result confirms the gradual weight loss occurring until 500°C. TG and DTA thermograms of 4CMIF are shown in Figure 10.

4.11 Thermodynamic Property Analysis in Gas Phase

On the basis of vibrational analysis, thermodynamic parameters like heat capacity (C°p.m), entropy (S°m) and enthalpy changes (ΔH°m) for 4CMIF molecule have been computed from the theoretical harmonic frequencies and tabulated in Table 12. Computed thermodynamic parameters increase with increase in temperature ranging from

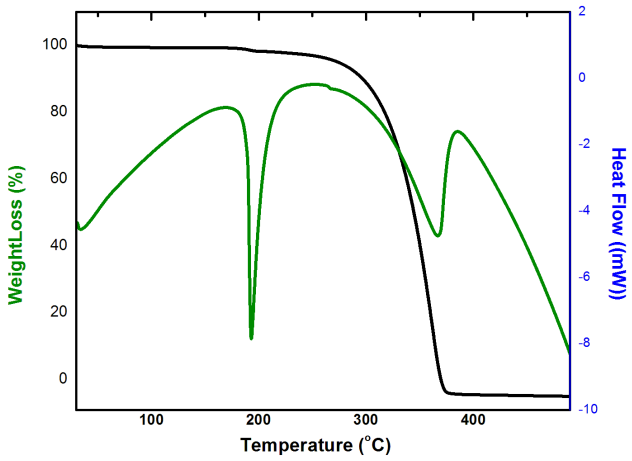

Figure 10. TG-DTA Thermograms of 4CMIF.

Table 12. Thermodynamic parameters of 4CMIF

Temperature T (K)	Heat Capacity Cpcal/mol.k	Entropy S (Cal/mol.K)	Enthalpy ΔH(kCal/mol)
100	32.76251	91.66909	2.020637
200	55.58185	121.456	6.448842
298.15	77.41238	147.738	12.98128
300	77.81364	148.218	13.124588
400	98.20631	173.467	21.949947
500	115.246	197.277	32.652637
600	128.922	219.545	44.886329
700	139.875	240.272	58.345301
800	148.753	259.549	72.793095
900	156.048	277.506	88.043413
1000	162.107	294.27	103.96011

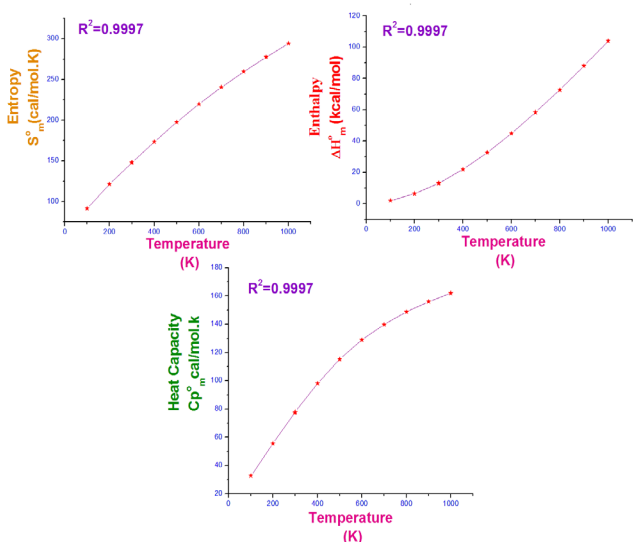

Figure 11. Thermodynamic Parameters of 4CMIF.

100 to 1000 K due to the fact that, the molecular vibrational intensities increase with increase in temperature[45]. Correlation equations between heat capacity, entropy, enthalpy changes and temperatures were fitted by quadratic formulas and the corresponding fitting factors (R^2) for these thermodynamic properties are 0.9997. Thermochemical field uses these parameters to compute the other thermodynamic energies and estimate directions of chemical reactions according to relationships of thermodynamic functions using second law of thermodynamics[45].Results have been obtained by considering the molecule to be at room temperature 298.15 K and at 1 atmospheric pressure. All thermodynamic property calculations have been performed in gas phase. The correlation graphics are shown in Figure 11 and corresponding fitting equations (1-3) are as follows

$$C°p.m = 5.68 + 0.278T - 0.00001T2 \ (R^2 = 0.999) \ldots\ldots (1)$$

$$S°m = 62.32 + 0.308T - 0.00008T2 \ (R^2 = 0.999) \ldots\ldots (2)$$

5. Conclusion

4CMIF molecule exists in monoclinic system with $P2_1/c$ space group. Analyzed results by applying B3LYP/6-311++G(d,p) computations using Gaussian'09 program package climaxes simulated geometric parameters showing good correlations with the crystallographic bond parameters. PES scan performed reveals all possible conformations of 4CMIF.Spectroscopic and electronic

features of 4CMIF performed experimentally agree quite well with DFT data. Spectral analysis confirms lowering of C=O stretching frequency by intra-molecular hydrogen bonding effect while the protons attached to methyl group resonate at lower field confirmed by NMR spectra. Molecular electrostatic potential surface analysis identifies reactivity sites by mapping the electron density. TG-DTA result reveals that this sample can be utilized for opto-electronic and photonic device applications up to 300°C. Thermodynamic parameters; free energy change (ΔG), enthalpy change (ΔH), and entropy change (ΔS) have been computed to interpret the binding modes.

6. References

1. Aarushi G, Sahoo PK, Tejpal A. Genistein. A Potential Boon for Cancer Therapy. The Pharma Innovation Journal. 2016 May; 5(6):81–6.
2. Harborne JB. The Flavonoids: Advances in Research Since 1986. New York: Chapman & Hall; 1994. Crossref PMid:7765655
3. Polkowski K, Mazurek A P. ActaPoloniaePharmaceutica - Drug Research. 2000. p. 57–135.
4. Ren MQ, Kuhn G, Wegner J, Chen J. Isoflavones, substances with multi-biological and clinical properties. European Journal of Nutrition. 2001 Aug; 40:4. Crossref
5. Sundius T. Scaling of ab initio force fields by MOLVIB. VibrationalSpectroscopy. 2002 Jul; 29(1-2):89–95. Crossref
6. Sundius T. MOLVIB – A Flexible Program for Force Field Calculations. Journal of Molecular Structure.1990; 218:321–6. Crossref
7. Pulay P, Fogarasi G, Pongor G, Boggs JE, Vargha A. Combination of theoretical ab initio and experimental information to obtain reliable harmonic force constants. Scaled quantum mechanical (QM) force fields for glyoxal, acrolein, butadiene, formaldehyde, and ethylene. Journal of American Chemical Society.1983 Nov; 105:7037–47. Crossref
8. Pulay P, Fogarasi G, Pang F, Boggs JE. Density Functional Analysis of Anharmonic Contributions to Adenine Matrix Isolation Spectra. Journal of American Chemical Society. 1979; 101:2550–60. Crossref
9. Natural Bond Orbital Analysis. Available from Crossref
10. Yoosefian M, Etminan N. The role of solvent polarity in the electronic properties, stability and reactivity trend of a tryptophane/Pd doped SWCNT novel nano biosensor from polar protic to non-polar solvents. Journal of the Royal Society of Chemistry. 2016 Jul; 6:64818–25. Crossref
11. Scott AP, Random L. Harmonic vibrational frequencies: an evaluation of Hartree-Fock, Moller-Plesset, Quadric Configuration Interaction, Density Functional Theory, and Semiempirical Scale Factors. Journal of Physical Chemistry. 1996; 100(41):16502–13. Crossref
12. Karabacak M, Kose E, Ata A. Molecular structure (monomeric and dimeric structure) and HOMO-LUMO analysis of 2-aminonicotinic acid: a comparison of calculated spectroscopic properties with FT-IR and UV-vis. SpectrochimicaActa Part A. 2012 Jan; 91:83–96. Crossref PMid:22366618
13. Westrip SP. publCIF: software for editing, validating and formatting crystallographic information files. Journal of Applied Crystallography. 2010 Aug; 43(4):920–5. Crossref
14. Sawant AB, Nirwan RS. Synthesis, characterization and DFT studies of 6.8-dichloro-2-(4-Chlorophenyl)-4H-Chromene-4-one. Indian Journal of Pure & Applied Physics. 2012 May; 50:308–13.
15. George JA. An introduction to hydrogen bonding. Oxford University Press; 1997.
16. Pauling L. The nature of the chemical bond. New York: Cornell University Press; 1960. PMid:16590757, PMCid:PMC223050
17. Bellamy LJ. The infrared spectra of complex molecules. London: Chapmann & Hall; 1975. Crossref PMCid:PMC470331
18. Roeges NPG. A Guide to the Complete Interpretation of Infrared Spectra of Organic Structures. New York: Wiley; 1994.
19. Rehman S. Synthesis, characterization, in vitro antimicrobial, and U2OS tumoricidal activities of different coumarin derivatives. Chemistry Central Journal. 2013 Apr; 7(1):7–68. Crossref PMid:23587363 PMCid:PMC3668295
20. Silverstein M, Clayton Basseler G, Morril C. Spectrometric Identification of Organic Compounds. New York: Wiley; 1981.
21. Varsanyi G. Vibrational Spectra of Benzene Derivatives. New York: Academic Press; 1969.
22. Ahluwalia VK. Textbook Of Organic Chemistry. A1 Books Pvt Ltd; 2010.
23. Scheiner, Grabowski S, Kar SJ. Influence of Hybridization and Substitution on the Properties of the CH...O hydrogen Bond. Journal of Physical Chemistry A. 2001; 105(46):10607–12. Crossref
24. Sahoo S, Chakraborti CK, Mishra SC. FTIR and Raman Spectroscopic Investigations Of Controlled Release Ofloxacin / HPMC Mucoadhesive Suspension. International Journal of Pharmacy & Technology. 2011 Jun; 3(2):2420–39.
25. Grabowski SJ. Hydrogen Bonding - New Insights. Dordrecht; Springer: 2006. Crossref
26. Mooney EF. The infra-red spectra of chloro- and bromobenzene derivatives—II. Nitrobenzenes, SpectrochimicaActa. 1964 Jun; 20:1021–32. Crossref

27. Kurt M, Babu CP, Sundaraganesan N, Cinar M, Karabacak M. Molecular structure, vibrational, UV and NBO analysis of 4-chloro-7-nitrobenzofurazan by DFT calculations. SpectrochimicaActa Part A. 2011 Sep; 79:1162–70. Crossref PMid:21571581
28. Smith B. Infrared Spectral Interpretation-A Systematic Approach. New York: CRC Press; 1999.
29. Durig JR. Vibrational Spectra Structure: A Series of Advances. New York: Elseiver Scientific Publications; 1975.
30. Girijavallabhan CP, Venkateswarlu K. Raman Spectrum of Coumarin. Current Science. 1968 Jan; 10.
31. Venkateswaran CS. Raman Effect and Molecular Structure. Current Science. 1937 Jul; 6:5.
32. Uesugi Y, Mizuno M, Shimojima A, Takahashi H. Transient Resonance Raman And Ab-Initio Mo Calculation Studies Of Thestructures And Vibrational Assignments Of The T-1 State And The Anion-Radical Of Coumarin And Its Isotopically Substituted Analogs. Journal of Physical Chemistry A. 1997; 101:268–74. Crossref
33. Sortur V, Yenagi J, Tonnavar L, Jadhav LB, Kulkarni MV. Vibrational assignments for 7-methyl-4-bromomethylcoumarin, as aided by RHF and B3LYP/6-31G* calculations. SpectrochimicaActa Part A: Molecular and Biomolecular Spectroscopy. 2008 Nov; 71(2):688–94. Crossref PMid:18329952
34. Ravikumar C, Joe I H, Jayakumar VS. Charge transfer interactions and nonlinear optical properties of push–pull chromophore benzaldehyde phenylhydrazone: A Vibrational Approach. Chemical Physics Letters. 2008; 460:552–8. Crossref
35. Mohan J. Organic Spectroscopy Principles and Applications. New Delhi: Narosa Publishing House; 2009.
36. Fukui K. Role of frontier orbitals in chemical reactions. Science. 1982 Nov; 218:747–54. Crossref PMid:17771019
37. Amalanathan M, Joe IH, Rastogi VK. Molecular structure, Vibrational spectra and nonlinear optical properties of L-Valine Hydrobromide: DFT study. Journal of Molecular Structure. 2011 Jan; 985(1):48. Crossref
38. Thirupugalmani K, Karthick S, Shanmugam G, Kannan V, Sridhar B, Nehru K, Brahadeeswaran S. Second- and third-order nonlinear optical and quantum chemical studies on 2-amino-4-picolinium-nitrophenolate-nitrophenol: A phasematchable organic single crystal. Optical Materials. 2015 Nov; 49:158–70. Crossref
39. Sheela GE, Manimaran D, Joe HI, Rahim S, Jothy BV. SpectrochimicaActa Part A: Molecular and Biomolecular Spectroscopy. 2015 Feb; 143:40. Crossref PMid:25710113
40. Sharma YR. Elementary Organic Spectroscopy Principles and Chemical Applications. New Delhi: S. Chand & Company LTD; 2008.
41. Mabry TJ, Markham KR, Thomas MB. The Systematic Identification of Flavonoids. 1970.
42. Sharma BK. Spectroscopy. Meerut: Goel Publishing House; 2011.
43. Jacobsen NE. NMR Data Interpretation Explained: Understanding 1d and 2D NMR Spectra of Organic Compounds and Natural Products. Wiley; 2016.
44. Kalinowski HO, Berger S, Braun S. Carbon-13 NMR Spectroscopy. Chichester: John Wiley & Sons; 1988.
45. Ott BJ, Boerio-goates J. Calculations from Statistical Thermodynamics. Academic Press; 2000.